Journal of the European Ceramic Society 23 (2003) 737–744
www.elsevier.com/locate/jeurceramsoc

New spinel-containing refractory cements

A.H. De Aza[a], P. Pena[a], M.A. Rodriguez[a], R. Torrecillas[b], S. De Aza[a,*]

[a]*Instituto de Cerámica y Vidrio, CSIC. Arganda del Rey, 28500 Madrid, Spain*
[b]*Instituto Nacional del Carbón, CSIC. La Corredoría s/n, 33080 Oviedo, Spain*

Received 8 December 2001; received in revised form 10 May 2002; accepted 17 May 2002

Abstract

Use of spinel-containing high alumina refractory concretes has increased significantly over the last few years. Currently the high cost of sintered or electrofused spinels limits their applications. This paper describes new and inexpensive new spinel-containing refractory cements obtained by a reaction-sintering process between dolomite and alumina. The reaction-sintering process occurs in two well defined steps: (a) reaction and (b) sintering. The reaction also happened in two successive stages: (a) dolomite decomposition in the range 700–900 °C, and (b) reaction of lime and magnesia with alumina, in the range from 900 to 1250 °C. A selected composition containing: 43±5 wt.% $CaAl_2O_4$, 15±3 wt.% $CaAl_4O_7$ and 42±2 wt.% $MgAl_2O_4$, showed a hydration and dehydration behaviour similar to that of commercial calcium aluminate cements. The evolution of the hydrated pure $CaAl_2O_4$ cement up to 1500 °C has also been studied.

Keywords: AlO_3; Calcium aluminate cements; Dolomite; $MgAl_2O_4$; Refractory cements; Spinel

1. Introduction

Alumina refractory materials with additions of synthetic spinel ($MgAl_2O_4$) have attracted increasing interest in recent years due to their good refractory performance in many technological applications (e.g. cement and concrete industry, glass industry and iron and steel industry). Moreover, the progress in steelmaking technology involves the development of processes with higher temperatures and longer holding times with particular emphasis on steel ladle linings and clean steel requirements. In this way, it was found that spinel additions performed particularly well in steelmaking refractories.[1,2]

Early trials carried out in pilot plants in Japan[3,4] showed that alumina-spinel castables at ladle side walls gave two to three times longer life than a castable containing 70 wt.% zircon. Alumina-spinel castables at the ladle bottom were shown to have five times the durability of roseki bricks, while at the impact pad the castable only has 20–30% of the durability of roseki brick.

Additionally, spinel was found to impart to the castables improved resistance to both thermomechanical stress and slag attack. The spinel takes into solid solution large amount of bivalent and trivalent elements (e.g. Mn^{+2}, Fe^{+2}, Fe^{+3}, Cr^{+3} ...) from the slag, changing the composition of this, making it more viscous and compatible with the spinel-alumina castable and diminishing considerably slag penetration into it.[5–8] On the other hand, the use of alumina-spinel refractory castables in ladles has improved the quality of the steel since it avoids the silica contamination coming from the alumina–silica and zircon refractory materials.

Summarising, the use of spinel in matrices in high alumina castables confers excellent durability in steel ladles. However, at the present time, the high cost of the sintered and electrofused spinels represents a handicap to more extended development of this kind of refractory materials. Consequently, the aim of the present work is to develop new refractory cements, already containing spinel, by means of an innovative and economically profitable reaction-sintering process between dolomite [$CaMg(CO_3)_2$] and alumina mixtures.

2. Theoretical design of the new cements

Although the mineralogy of calcium aluminate refractory cements may vary considerably, one of the

* Corresponding author. Tel.: +34-1-871-1800; fax: +34-1-870-0550.
E-mail address: aza@icv.csic.es (S. De Aza).

0955-2219/02/$ - see front matter © 2002 Published by Elsevier Science Ltd.
PII: S0955-2219(02)00166-8

essential characteristics of these cements is that they are fundamentally constituted by calcium monoaluminate ($CaAl_2O_4$), which is the main phase responsible for the hydraulic hardening of the cement. Thus, taking into account the solid state compatibilities in the system Al_2O_3–MgO–CaO[9,10] (Fig. 1), new cements containing calcium monoaluminate ($CaAl_2O_4$) and spinel ($MgAl_2O_4$), as main phases, with calcium dialuminate ($CaAl_4O_7$) as an additional hydraulic phase, can be obtained by reaction-sintering of dolomite and alumina. So, any mixture giving the mentioned group of phases must be located within their subsystem in the segment A–B (Fig. 1) of the line that join *doloma* (CaO·MgO) and alumina. All these compositions, considering a theoretical dolomite, are given by the following general equation:

$$(1+y)\ Al_2O_3 + [0.5\ MgO\ 0.5CaO] \rightarrow (0.5-y)\ CaAl_2O_4 + yCaAl_4O_7 + 0.5MgAl_2O_4 \quad (1)$$

where $0 \leqslant y \leqslant 0.5$

From all these possible compositions, the selected one must be among those giving a proportion of $CaAl_2O_4$ (the main hydraulic phase of the cement) in the range 40–45 wt.% and having, as far as possible, the maximum content of $MgAl_2O_4$. Thus, the composition selected was that one with a y value equal to 0.075. This composition completely reacted and in equilibrium condition in the solid state, will be constituted by: 42.56 wt.% $CaAl_2O_4$, 45.08 wt.% $MgAl_2O_4$ and 12.36 wt.% $CaAl_4O_7$.

On the other hand, the invariant peritectic point of the subsystem $CaAl_2O_4$–$MgAl_2O_4$–$CaAl_4O_7$ takes place at 1567±2 °C (Fig. 1). Due to its location, for all the compositions within the mentioned subsystem, calcium monoaluminate ($CaAl_2O_4$) will be the first phase to disappear by dissolution in the liquid phase as soon as the temperature of the invariant point is exceeded. Consequently, the reaction-sintering process between dolomite and alumina must be carried out at temperatures lower than 1567±2 °C.

3. Experimental procedure

The raw materials used in this investigation were: alumina CT 3000SG (Alcoa, Pittsburgh, PA, USA) and a finely milled mineral dolomite [$CaMg(CO_3)_2$] supplied by Prodomasa (Productos Dolomíticos de Málaga, Coin, Málaga, Spain). The alumina had an average particle size of 0.4 μm (by laser diffraction), a surface area of 8 m^2/g (by B.E.T.) and a purity ⩾99.6 wt.%

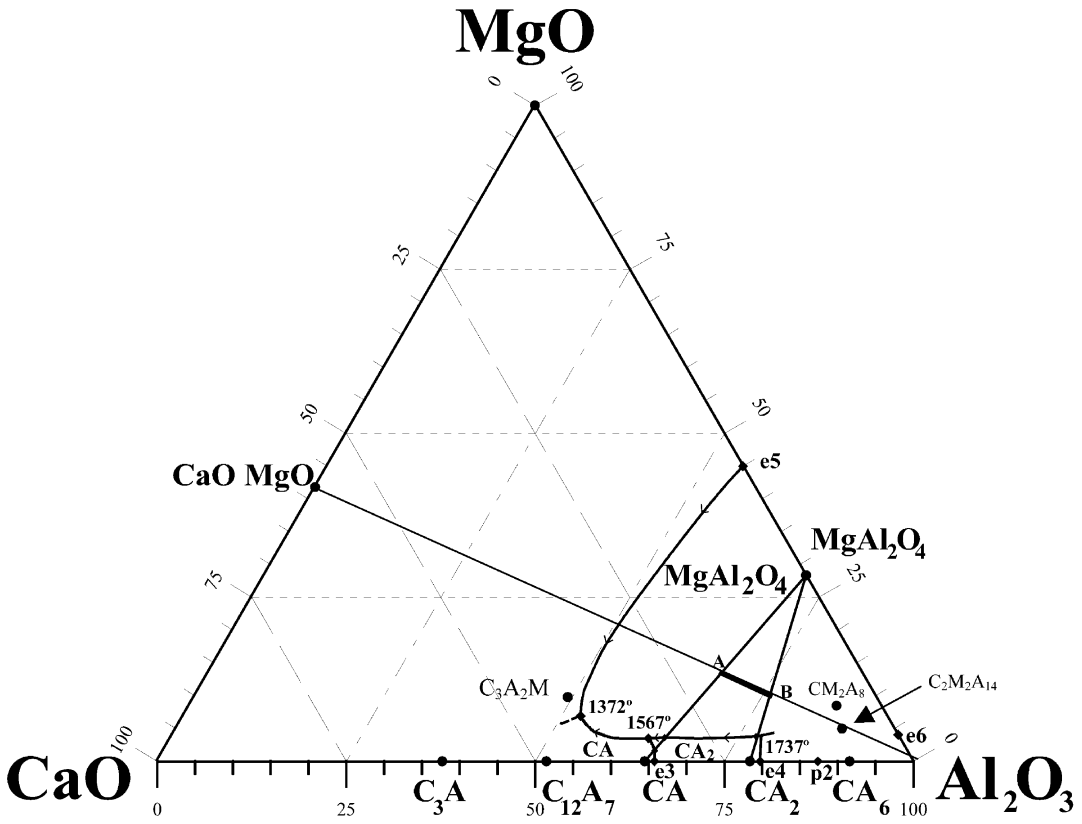

Fig. 1. Simplified Al_2O_3–MgO–CaO system,[9,10] showing the subsystem $CaAl_2O_4$–$MgAl_2O_4$–$CaAl_4O_7$ and the line that joint the *doloma* (CaO·MgO) and alumina (Al_2O_3). Cement notation is used in the figure; i.e., C is CaO, M is MgO, and A is Al_2O_3 (e.g., CA_6 is $CaO{\cdot}6Al_2O_3$ or $CaAl_{12}O_{19}$).

Table 1
Chemical analysis of the dolomite

Analytical method	Species	Content	Theoretical composition (wt.%)
Gravimetry	CaO	30.3±0.1 wt.%	30.41
Gravimetry	MgO	22.1±0.1 wt.%	21.83
Ignition loss		47.75±0.03 wt.%	47.73
ICP[a]	Al_2O_3	110 ppm ±10	–
	SiO_2	180 ppm ±15	–
	Fe_2O_3	80 ppm ±5	–
	TiO_2	14 ppm ±5	–
	SrO	47 ppm ±8	–
	MnO	traces	–
	P_2O_5	59 ppm ±20	–
	Nb_2O_5	13 ppm ±5	–
F. Ph[a].	Na_2O	18 ppm ±5	–

[a] ICP = Inductively couple plasma; F. Ph. = flame photometry.

Al_2O_3 being the main impurities: MgO ~ 0.09 wt.% and Na_2O ~ 0.09 wt.% (by ICP–AES and flame photometry respectively). The Prodomasa dolomite is one of the purest in the world and its chemical composition is shown in Table 1. This material had an average particle size of 4.9 μ (by laser diffraction) and a surface area of 2.5 m^2/g (by B.E.T.).

The composition selected was prepared by mixing the appropriate proportions of Al_2O_3 and $CaMg(CO_3)_2$ given by Eq. (1) where $y = 0.075$. A 50 wt.% solids suspension of the mixture with an optimum addition of 1 wt.% of an alkali-free polyelectrolite (Dolapix PC 33, Zschimmer & Schwarz, Lahnstein, Germany) was made to provide maximum stability of the aqueous dolomite-alumina suspension.[11] This was homogenised in an alumina mill with alumina balls for 14 h, proceeding later on to their drying in a plaster of Paris mould. The compact material obtained in this way was used to study the reaction-sintering process. Differential thermal analysis and thermogravimetry (DTA and TG, Netzsch STA 409); dilatometric analysis (Adamel-Lhomargy DI-24) and X-ray diffraction techniques (DRX, Siemens D 5000, Kristalloflex 710, K_α = Cu, Ni filter) were used to study the reaction-sintering process. To support the reaction mechanism, thermodynamic calculations were performed using the HSC computation package.[12]

Isothermal treatments were achieved for different times at temperatures ranging from 900 to 1500 °C. A constant heating rate of 5 °C/min up to the selected temperature was used.

Once the reaction mechanism was established, one kilogram of the cement was obtained at 1450 °C for 2 h, using the same thermal cycle that was described above. The final phase composition was determined by quantitative X-ray diffraction analysis.[13] The microstructure was studied on diamond polished samples (up to 1 μm) by scanning electron microscopy (SEM) using a C. Zeiss DSM-950 fitted wit an energy-dispersive spectrometer (EDS, Tracor Northern).

The amount of water required for the hydration of the cement was determined using the Ball-in-Hand Test.[14] A water cement ratio (w/c) of ≈0.4 was determined and considered as appropriate. Prismatic bars of 10×10×60 mm of pure $CaAl_2O_4$ cement were obtained using a metallic mould in which the cement paste was placed with the appropriate w/c ratio. The samples were vibrated until all the air bubbles emerged from the cement and its upper surface were smooth. Subsequently, the cement was cured at 20 °C in an atmosphere controlled chamber with a relative humidity atmosphere of 90%. The hydration and dehydration behaviour and porosity evolution versus temperature has also been studied using the above mentioned techniques (DTA–TG, dilatometry and XRD) from room temperature up to 1500 °C.

4. Results and discussion

4.1. Non-isothermal study of the reaction-sintering process

When the selected dolomite-alumina mixture was subject to thermal treatment at a constant heating rate, several phenomena were observed by DTA, TG and XRD.

The DTA plots recorded at 5 and 10 °C/min are shown in Fig. 2a. Both curves exhibit three endothermic effects: the first one, very broad, with a minimum at ~120 °C is attributed to a loss of free water, while the second (~775 °C) and the third peak (~900–925 °C) correspond to the decomposition of the dolomite according to Otsuka[15] and De Aza et al.[16] The DTA curve of the sample recorded at 5 °C/min shows a sharp exothermic peak at ≈950 °C, while in the DTA curve at 10 °C/min that peak overlaps with the broad endothermic calcite peak. However, this curve presents a small exothermic effect at ~1120 °C which is not detected in the DTA curve at 5 °C/min. The TG recorded at 5 °C/min (Fig. 2b) shows clearly the weight loss of free water and CO_2 which correspond to the endothermic peaks shown in the DTA curves. The sample presents a significant weight loss of ~22 wt.%.

The constant heating rate dilatometric curve (Fig. 2c) and its derived curve (Fig. 2d) show, apart of the shrinkage effects corresponding to the dolomite decomposition, three significant expansible effects at ~950, ~1100 and ~1200 °C, attributed to the formation of $CaAl_2O_4$, $MgAl_2O_4$ and $CaAl_4O_7$ respectively. At temperatures higher than 1250 °C, the predominant effect is sample shrinkage: initially in the solid state and later

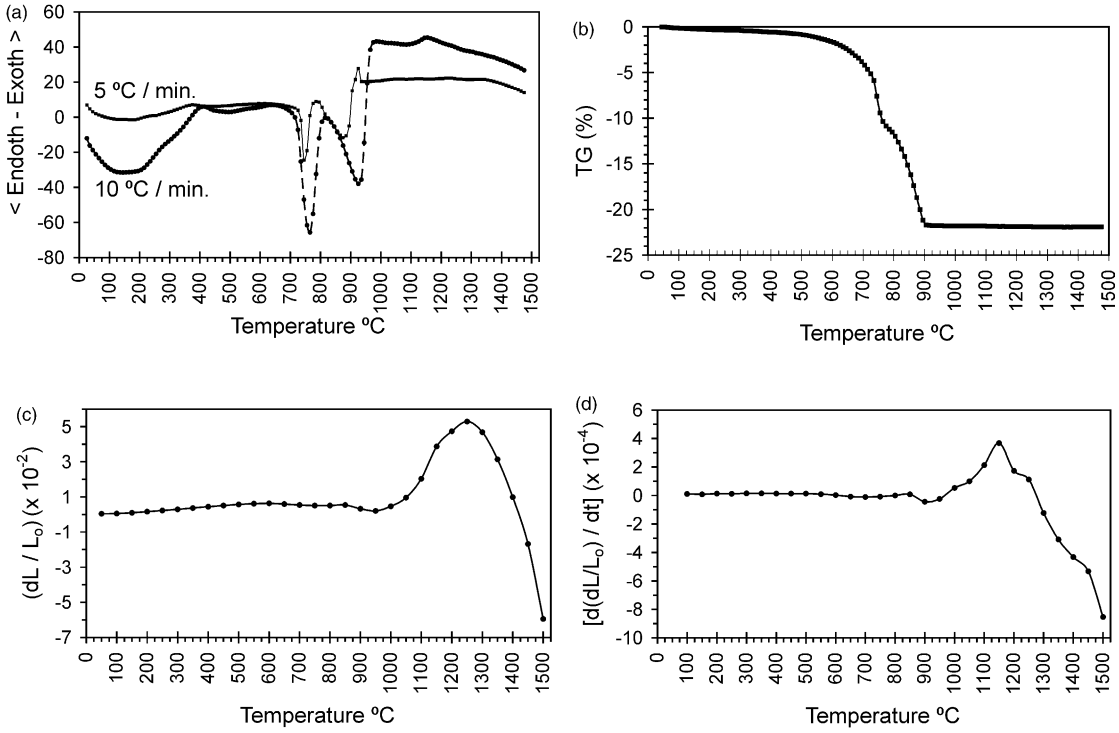

Fig. 2. (a) DTA's of the dolomite-alumina mixture with $y = 0.075$. (b) TG of the same sample at 5 °C/min. (c) Its dilatometric curve at 5 °C/min and (d) derived dilatometric curve versus temperature.

(~1450 °C) in the presence of a liquid phase due to the impurities contributed by the dolomite (Fig. 2d).

The results of XRD are summarised in Table 2. This shows phase evolution with temperature in the range 900–1500 °C with a holding time at each temperature of 0.1 h. CaO is known to easily react with the moisture in the air to form $Ca(OH)_2$, hence its presence in the XRD patterns.

The Gibbs energy (ΔG) and the enthalpy of formation (ΔH) of the phases involved in the reaction in the range 900–1500 °C are shown in Fig. 3a and b respectively. The changes in volume, that implies these reactions, were also calculated (Table 3).

With all the above information, the mechanism of the reaction-sintering process, in the range 700–1500 °C can be established as follows:

Table 2
Phase evolution versus temperature

Temperature	Al_2O_3	MgO	$Ca(OH)_2$ CH_2	$CaAl_2O_4$ CA	$CaAl_4O_7$ CA_2	$MgAl_2O_4$ Ma
900 °C	XXX	XXX	XX	X	–	–
950 °C	XXX	XXX	XX	X	–	–
1000 °C	XXX	XXX	XX	XX	–	?
1100 °C	XX	XX	X	XX	–	X
1200 °C	X	X	–	XX	?	X
1300 °C	–	–	–	XX	X	XX
1350 °C	–	–	–	XX	XX	XX
1450 °C	–	–	–	XXX	XXX	XXX
1500 °C	–	–	–	XXX	XXX	XXX

XXX Very Abundant; XX Abundant; X Scarce; ? Do not present? It can be present in small quantities, but the detection limit of this technique and the overlapping of its characteristic diffraction lines with other present phases does not allow to confirm it.

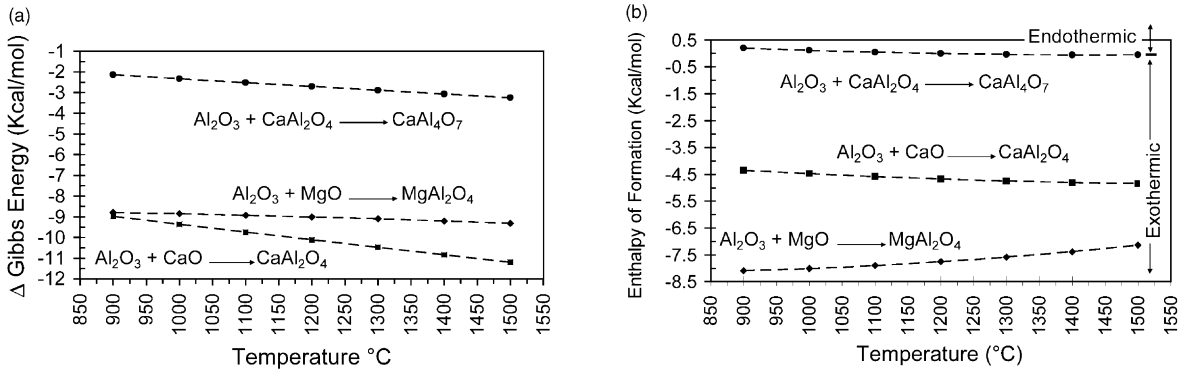

Fig. 3. (a) Evolution with temperature of the Gibbs energy (ΔG) and (b) enthalpy of formation (ΔH) of the phases involved in the reaction.

Table 3
Changes in volume that implies the following reactions.

Reaction	ΔV (en %)
$CaO + Al_2O_3 \rightarrow CaAl_2O_4$	+24.49%
$Al_2O_3MgO \rightarrow MgAl_2O_4$	+9.3%
$Al_2O_3 + CaAl_2O_4 \rightarrow CaAl_4O_7$	+13.6%

1. The dolomite decomposes first, in the temperature range from 700 to 900 °C, in the two following stages in agreement with previous data:[15,16]

$$CaMg(CO_3)_2 \overset{\approx 775^{\circ}C}{\rightarrow} CaMg_{(1-x)}(CO_3)_{(2-x)} + xMgO + xCO_2(g) \quad (2)$$

$$CaMg_{(1-x)}(CO_3)_{(2-x)} \overset{\approx 900^{\circ}C}{\rightarrow} CaO + (1-x)MgO + (2-x)CO_2(g) \quad (3)$$

where $0 \leqslant x \leqslant 1$.

2. At ~950 °C calcium monoaluminate ($CaAl_2O_4$) formation takes place by an expansive and exothermic reaction (see Figs. 2a and d and 3b and Tables 2 and 3). This $CaAl_2O_4$ formation is the reaction with the highest negative value of ΔG (Fig. 3a).

3. Between 1000 and 1100 °C the expansile and exothermic reaction of spinel ($MgAl_2O_4$) formation occurs (see Figs. 2d and 3b and Tables 2 and 3).

4. At ~1200 °C calcium dialuminate ($CaAl_4O_7$) is formed by an expansile and endothermic reaction (see Figs. 2d and 3b and Tables 2 and 3).

5. At temperatures higher than 1250 °C the sintering process occurs, first in the solid state and later in the presence of a liquid phase (Fig. 2c and d).

These results show that, in the reaction-sintering of the dolomite-alumina mixtures, the reaction occurs prior to densification. Chemical reaction of the reactants was completed at 1300 °C whereas at this temperature the porosity of the compact was 32% higher than the initial value (green density = 2.20 g/cm^3 and ρ_{1300} = 1.50 g/cm^3). The origin of the porosity in the reacted samples include such factors as the molar volume changes during reaction (Table 3) and CO_2 weight loss (~22 wt.%).

4.2. Isothermal study of the reaction-sintering process

With the aim of selecting the most appropriate temperature to proceed to the synthesis of the cement, an isothermal study of the process was carried out at different temperatures in the range 1300–1500 °C, at which the three main phases of the new cement ($CaAl_2O_4$, $MgAl_2O_4$ and $CaAl_4O_7$) have already formed, holding 2 h at each temperature. The maximum temperature of 1500 °C was selected due to the presence of dolomite impurities. These can reduce the theoretical maximum temperature of synthesis (1567±2 °C, see Fig. 1), as mentioned previously, giving place to the decrease or disappearance of the calcium monoaluminate ($CaAl_2O_4$) phase. After each thermal treatment, a semi-quantitative XRD analysis of the phases present as well as a microstructural study by SEM-EDS was made.

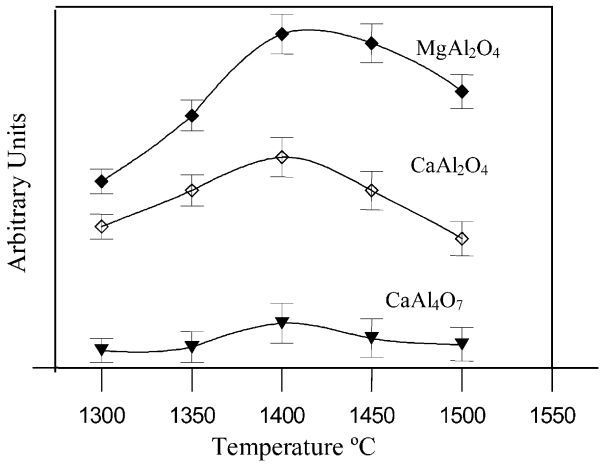

Fig. 4. Evolution of the different phases versus temperature in the range 1300–1500 °C. Holding times: 2 h.

The evolution of the different phases with temperature in the range 1300–1500 °C is shown in Fig. 4. As can be seen all the phases present a maximum around 1400 °C. Typical SEM images of the samples heated a 1400 and 1450 °C/2 h respectively are shown in Fig. 5. The samples treated at 1400 °C/2 h are porous with small (<1 μm) grain size of the crystalline phases. However, the sample treated at 1450 °C/2 h shows low porosity and an average grain size of ~2.5 μm. No glassy phase was detected in both samples by TEM. To distinguish between $CaAl_2O_4$ and $CaAl_4O_7$ EDS analyses were necessary because both phases present similar contrast.

These results suggested the thermal treatment of 1450 °C/2 h for cement synthesis. Then, a second batch of one kilogram of cement was prepared. A typical microstructure of the obtained cement is shown in Fig. 6. The proportion of the different phases in the new cement was determined by quantitative XRD analysis and the results are shown in Table 4 revealing a good correlation between the theoretical and experimental values.

The clinker of the cement was milled in tungsten carbide mill and sieved 60 μm. It had an average particle size of 4.2

Table 4.
Quantitative analysis of the obtained cement (wt.%).

New Cement	$MgAl_2O_4$ MA	$CaAl_4O_7$ CA_2	$CaAl_2O_4$ CA
Theoretical	45.08	12.36	42.56
Obtained at 1450 °C/2 h	42±2	15±3	43±5

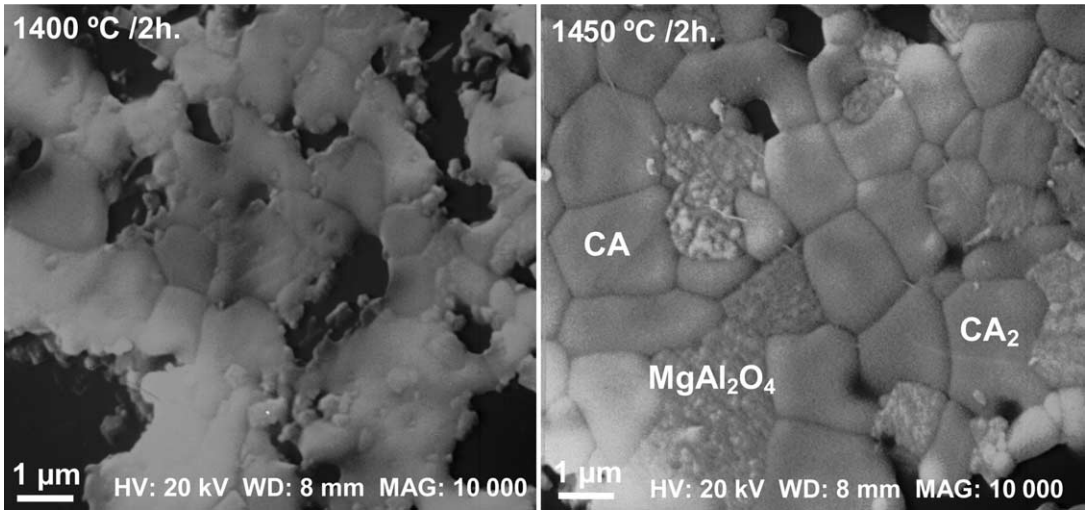

Fig. 5. SEM micrographs of the microstructure of the samples treated at 1400 °C (left) and 1450 °C (right).

Table 5.
Evolution of the different phases during the hydration–dehydration–re-crystallisation process

Temperature	CA $CaAl_2O_4$	MA $MgAl_2O_4$	CA_2 $CaAl_4O_7$	$C_{12}A_7$ $Ca_{12}Al_{14}O_{33}$	CAH_{10} $CaAl_2O_4$ $10H_2O$	C_3AH_6 $Ca_3Al_2O_6$ $6H_2O$	AH_3 $Al(OH)_3$
Anhydrous Cement	X	X	X	–	–	–	–
20 °C. w/c = 0.4	X	X	X	–	X	–	–
260 °C	–	X	–	–	–	X	X
450 °C	–	X	–	X	–	–	–
800 °C	–	X	–	X	–	–	–
1000 °C	X	X	X	X	–	–	–

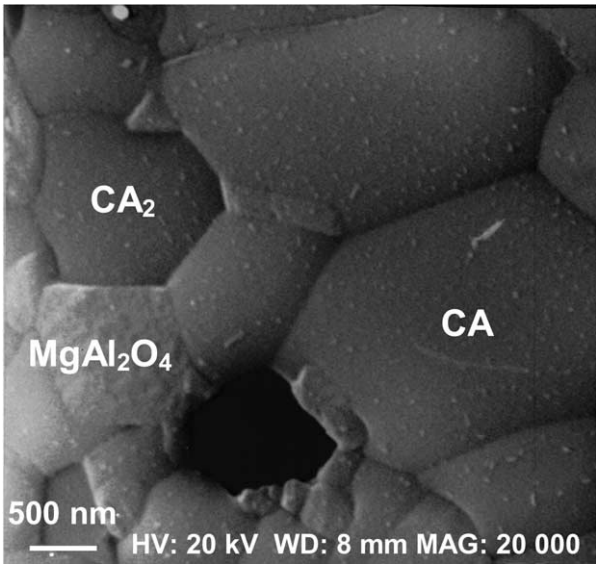

Fig. 6. Typical SEM micrograph of the microstructure of the cement obtained.

µm (by laser diffraction), a surface area of 2.6 m^2/g (by B.E.T.) and a true density of 3.1 g/cm^3 (by He picnometer).

4.3. Hydration and dehydration behaviour versus temperature

Hydrated samples, as described in the experimental procedure, were studied by DTA and TG (Fig. 7a and b) and dilatometry (Fig. 7c and d) and, after heating and quenching at selected temperatures, by XRD (Table 5).

The cured cement under normal conditions produces the metastable phases $CaAl_2O_4{\cdot}10H_2O$ (CAH_{10}) and alumina gel; heating to 110 °C in air, converts the hydrated cement into a mixture of gibbsite ($Al(OH)_3 = AH_3$) and hydrogarnet ($Ca_3Al_2O_6{\cdot}6H_2O = C_3AH_6$). In the temperature range 300–400 °C, the most common and accepted interpretation of the endothermic peaks and mass losses is in terms of gibbsite (≈320 °C) and hydrogarnet (≈360 °C) decomposition giving boehmite

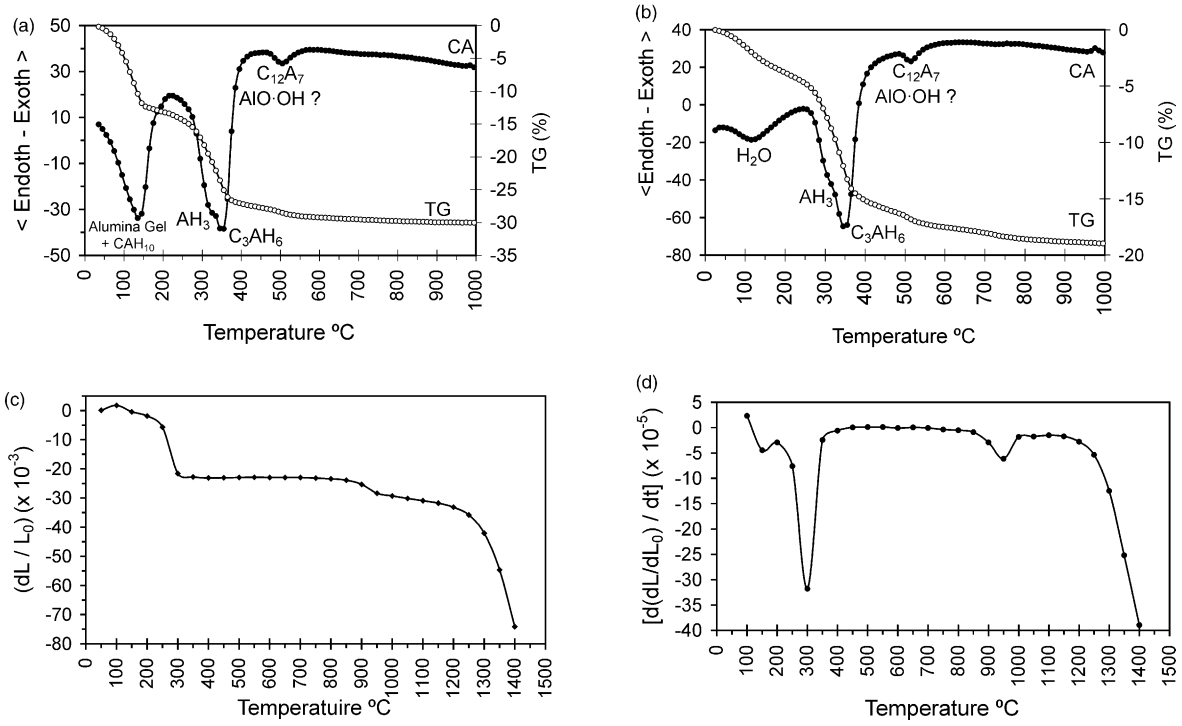

Fig. 7. (a) DTA–TG of the cement paste hydrated at 20 °C during 24 h. (b) DTA–TG of the converted cement. (c) Dilatometric curve of the cement paste hydrated at 20 °C during 24 h. (d) Derived dilatometric curve of the hydrated cement paste versus temperature.

or diaspore (AlO·OH) and amorphous alumina.[17,18] Heating to ~450 °C produces, according to MacKenzie et al.,[17] the diaspore decomposition and according to Nurse et al.,[19] Turrillas et al.[20] and the present results (Table 5), $Ca_{12}Al_{14}O_{33}$ ($C_{12}A_7$) formation. At ~950 °C a small exothermic peak in the DTA curve (Fig. 7a and b) indicates calcium monoaluminate formation (Table 5).

The TG and dilatometric data were used to construct a curve showing the variation of density versus temperature (Fig. 8). The criterion adopted to calculated the density at each temperature is given by the expression:

$$\rho_t = \frac{P_t}{L_t^3} = \frac{P_0(1+\Delta P)}{[L_0(1+\Delta L)]^3} = \rho_0 \frac{(1+\Delta P)}{(1+\Delta L)^3} = \frac{\rho_0}{(1+\Delta L)^3} + \frac{\rho_0 \Delta P}{(1+\Delta L)^3} \quad (4)$$

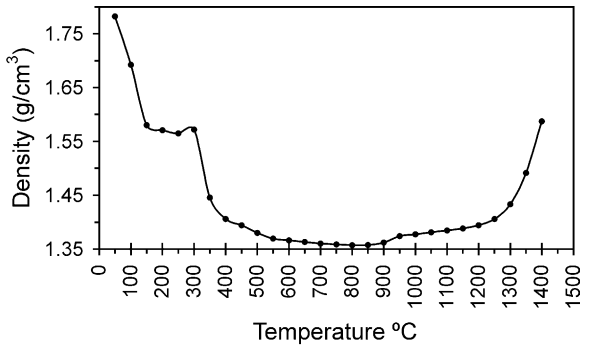

Fig. 8. Variation of density versus temperature of the hydrated cement.

where ρ is the density, P the weight, ΔP is the weight loss ($P_0 - P_t$) and L the length of the sample. The subindexes 0 and t denote that the value corresponds to room and to the selected temperature respectively. This kind of representation is new in the field of refractory cements and concretes and gives a graphic representation of the effects that the different processes of hydration, dehydration and sintering have on density. Between room temperature and ~250 °C there is a density decrease due to loss of free water and to dehydration and conversion of the metastable hydrates CAH_{10}, and AH_x gel. A decrease in density between 300 and 400 °C is attributed to the dehydration of the stable hydrates C_3AH_6 and AH_3. Around 500 °C a small density decrease also happens due to the continuous transformation of $Ca_{12}Al_{14}O_{33}$-like phase into $C_{12}Al_{14}O_{33}$.[18,20–22] It must be emphasised, however, that although there are some bibliographic data[17,18] showing the presence of diaspore (AlO·OH) in this range of temperature, nevertheless this phase has not been detected by XRD in the present study. Clearly, more work needs to be done in this region. From 500 to ~900 °C the density remains practically constant and at 900 °C small continuous increase of density until ~1250 °C is due to the initial solid state sintering and new formation of $CaAl_2O_4$ and $CaAl_4O_7$. Finally, above 1250 °C the density increases again first due to solid state sintering and later due to liquid phase sintering.

Therefore, the new cement behaves during hydration and dehydration much like traditional calcium aluminate cements.

Finally, although this work have been carried out using a particular dolomite (Prodomasa, Coin, Málaga, Spain) close to the theoretical stoichiometry, diverse spinel-containing calcium aluminate cements can be obtained within the subsystem $CaAl_2O_4$–$MgAl_2O_4$–$CaAl_4O_7$ with different proportion of phases, taking into account the following equation:[23]

$$(1+y)\ Al_2O_3\ + [(1-x)\ MgO \cdot x\ CaO] \rightarrow (x-y)\ CaAl_2O_4\ + yCaAl_4O_7 + (1-x)\ MgAl_2O_3 \quad (5)$$

where $0 \leqslant x \leqslant 1$ and $0 \leqslant y \leqslant x$.

5. Conclusions

New spinel-containing refractory cements can be achieved by reaction-sintering of dolomite and alumina mixtures.

The new cements behave as traditional calcium aluminate cements and can be used to produce spinel bonded high alumina refractory concretes, avoiding or reducing the use of expensive synthetic spinel.

A general equation based on the dolomite MgO/CaO molar ratio, that allows preparation of a range of cements with different proportions of the three main constituents: $CaAl_2O_4$, $MgAl_2O_4$ and $CaAl_4O_7$, has been established.

Acknowledgements

The authors thank to Prodomasa for kindly providing the dolomite from its quarries in Coin, Málaga, Spain. This work has been sponsored by MCyT under project MAT2000–0941.

References

1. O'Driscoll, M., *Spinel Review. Princes Temper Steel Market Promise*. Industrial Minerals, September 1994, pp. 35–49.
2. Lee, W. E. and Moore, R. E., Evolution of in situ refractories in the 20th century. *J. Am. Ceram. Soc.*, 1998, **81**(6), 1385–1410.
3. Nagai, B., Matsumoto, O. and Isobe, T., Development of monolithic refractory lining for BOF ladle in Japan mainly for the last decade. In *Global Advance in Refractories, Pre-prints, Unitecr'91 Congress,* ed. German Refract. Ass. and Inst. für Gesteinsshüttenkunfe, Aachen 1991, Germany, pp. 83–86.
4. Sumimura, H., Yamamura, T., Kubota, Y. and Kaneshige, T., Study on slag penetration of alumina-spinel castable. In *Global Advance in Refractories, Pre-prints, Unitecr'91 Congress*, ed. German Refract. Ass. and Inst. für Gesteinsshüttenkunfe, Aachen 1991, Germany, pp. 97–101.
5. Oguchi, Y. and Mori, J., Wear mechanism of castable for steel ladle. *Taikabutsu Overseas*, 1993, **13**(4), 43–49.
6. Korgul, P., Wilson, D. R. and Lee, W. E., Microstructural analysis of corroded alumina-spinel castable refractories. *J. Eur. Ceram. Soc.*, 1997, **17**, 77–84.
7. Domínguez, C., Raigón, M., Gómez, M., Ferrer, F. J., Pérez, E., De Aza, A. H., Caballero, A. and De Aza, S. Bottom working lining improvement in stainless steel ladles. UNITECR'2001. Hosted by ALAFAR. In *Proceedings of Unified International Technical Conference on Refractories. 7th Biennial Worldwide Congress*. Cancun, Mexico, 4–7 November. 2001, pp. 289–299.
8. Korgul, P., Wilson, D. R. and Lee, W. E., Microstructural analysis of corroded alumina-spinel castable refratories. *J. Eur. Ceram. Soc.*, 1997, **17**, 77–84.
9. De Aza, A. H., Pena, P. and De Aza, S., Ternary system Al_2O_3–MgO–CaO. Part I: primary phase field of crystallization of spinel in the subsystem: $MgAl_2O_4$–$CaAl_2O_7$–CaO–MgO. *J. Am. Ceram. Soc.*, 1999, **82**(8), 2193–2203.
10. De Aza, A. H., Iglesias, J. E., Pena, P. and De Aza, S., The system Al_2O_3–MgO–CaO. Part II: phase relationship in the subsystem Al_2O_3 $MgAl_2O_4$–$CaAl_4O_7$. *J. Am. Ceram. Soc.*, 2000, **83**(4), 919–927.
11. De Aza, A. H., Diseño y desarrollo de materiales de alta alúmina con matrices de espinela y hexaluminato cálcico (Design and development of high alumina materials with spinel and calcium hexaluminate in their matrices), Ph D thesis (in Spanish) Autonomous University of Madrid (UAM), Spain, 1997.
12. Outokumpu Research Oy, Pori, Finland, Outokumpu HSC Chemistry for Windows, Version 1.10. 1993.
13. Klug, H. P. and Alexander, L. E., *X-ray Diffraction Procedure for Polycrystalline and Amorphous Materials*, 2nd edn. John Wiley and Sons, New York, 1974.
14. Stardand practices for determining and measuring consistency of refractory concrete. ASTM designation C 860–91.
15. Otsuka, R., Recent studies on the decomposition of the dolomite group by thermal analysis. *Therm. Acta*, 1986, **100**, 69–80.
16. De Aza, A. H., Rodríguez, M. A., Rodríguez, J. L., De Aza, S., Pena, P., Convert, P., Hansen, T. and Turrillas, X., The decomposition of dolomite monitored by neutron thermodiffractometry. *J. Am. Ceram. Soc.*, 2002, **85**(4), 881–888.
17. Mackenzie, R. C., *Differential Thermal Analysis*, Vol. 1. Academic Press, 1970.
18. Majundar, A. J. and Roy, R., The CaO–Al_2O_3–H_2O system. *J. Am. Ceram. Soc.*, 1959, **39**, 434.
19. Nurse, R. W., Welch, J. H. and Majundar, A. J., The CaO–Al_2O_3 system in moisture-free atmosphere. *Trans. Brit. Ceram. Soc.*, 1965, **64**, 409–418.
20. Turrillas, X., Convert, P., Hansen, T., De Aza, A. H., Pena, P., Rodríguez, M. A. and De Aza, S., Dehydration of calcium aluminate hydrates investigated by neutron thermodiffractometry. In *Proceedings of the International Conference on Calcium Aluminate Cemets (CAC). Calcium Aluminate Cements 2001,* ed. R. J. Mangabhai and F. P. Glasser. 2001, pp. 517–531.
21. Bartl, H., Roentgen-Einkristallumtersuchungen an $(CaO)_3$ Al_2O_3 $(H_2O)_6$ und an $(CaO)_{12}(Al_2O_3)_7(H_2O)$. Neuer Vorschlag Zur 1/2 $(CaO)(Al_2O_3)_7$-Struktur. Neues Jahrbuch fuer Mineralogie. Monatshefte, 1969, p. 404.
22. Christensen, A. H., Neutron powder diffraction profile refinement studies on Ca11.3Al14O32.3 and CaC10(D0.88H0.12). *Journal of Solid State Chemistry*, 1984, **51**, 196.
23. De Aza, A. H., Pena, P., Torrecillas, R. and De Aza, S., Cementos refractarios aluminosos conteniendo espinela y procedimiento de obtención (Spinel-containing high alumina refractory cements and their obtained process) Spanish Patent, number: 2143369. January 2001.